

## WEEK 11: META-ANALYSES

Boris Bernhardt, PhD

Bratislav Misic, PhD

ORGA

LAST CLASS - PREPARE YOUR TALKS

10 MINUTES EACH

3 MINS Q&A

FINAL GRADE WILL BE BASED ON:  
IN CLASS PARTICIPATION  
MOCK GRANT PROPOSAL  
PRESENTATION

MERCURY: PLEASE RATE THE CLASS!

# SYSTEMATIC REVIEW & META-ANALYSES

SYSTEMATIC REVIEW:  
SUMMARY OF THE AVAILABLE EVIDENCE

META-ANALYSIS:  
STATISTICAL METHODS TO SYNTHESIZE FINDINGS

GOOD SRMAS  
INTERESTING BUT ADDRESSABLE RESEARCH QUESTION  
RIGOROUS AND TRANSPARANET METHODOLOGY  
SETTLES CONTROVERSIES AND DEFINE NEW HYPOTHESES

SUBSTANTIAL WORK  
RELATIVELY HIGH PAYOFF IF WELL DONE  
LOW DIRECT COST

# IDENTIFICATION OF A GOOD QUESTION

SOME A PRIORI 'INSIGHT' INTO THE LITERATURE

ITERATIVE APPROACH TO DEFINE/SPECIFY THE GOALS

STUDY SCREENING + SELECTION

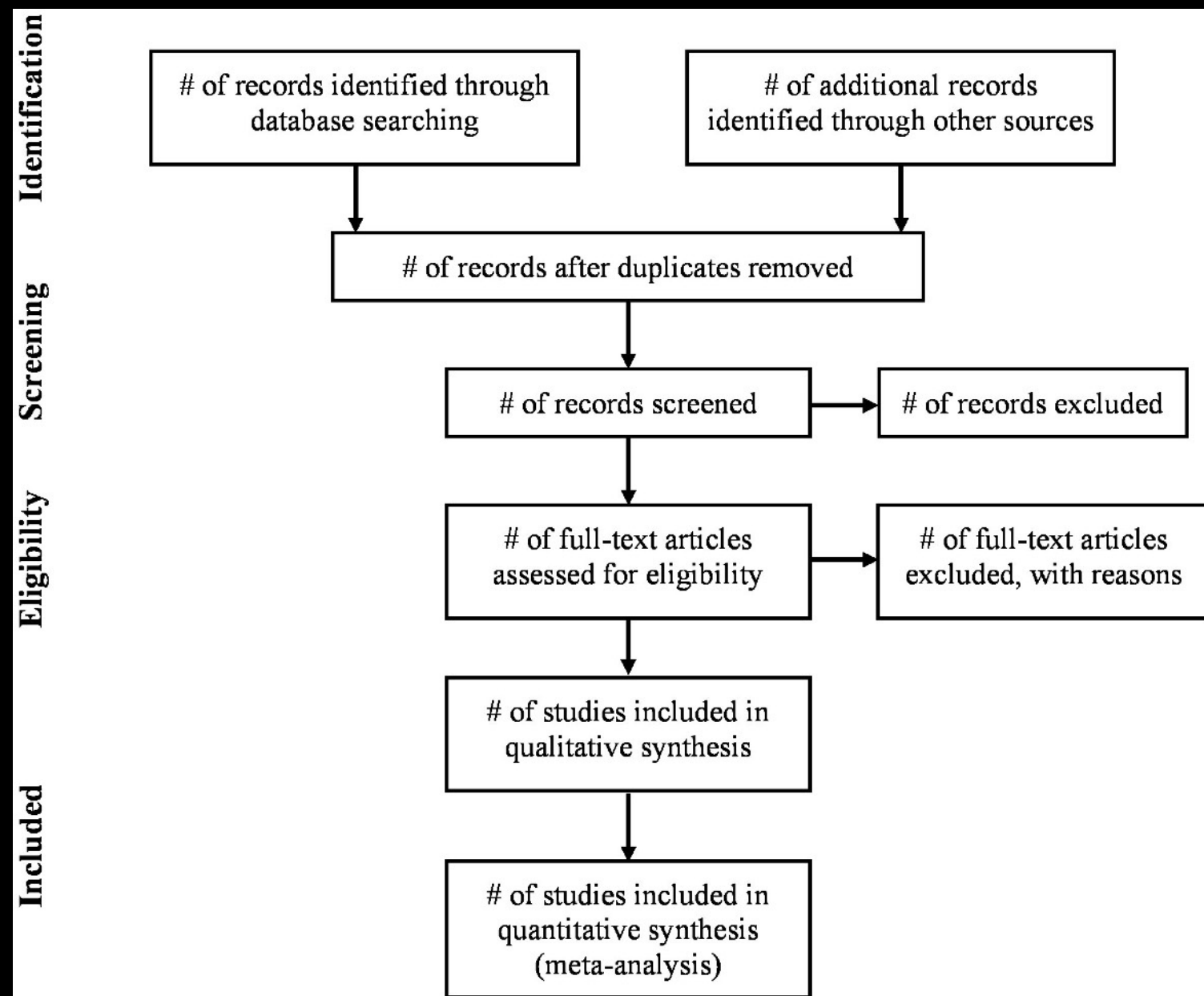
OVERALL GOAL:

REDUCE HETEROGENEITY THAT CANNOT BE MODELLED

GIVE OVERVIEW OF PREVIOUS STUDIES

EVALUATE BIAS (GARBAGE IN - GARBAGE OUT)

# STUDY IDENTIFICATION: THE PRISMA GUIDELINES



# COLLECTING EFFECT SIZE MEASURES + TRANSFORMING THEM

CORRELATION COEFFICIENTS

T-STATISTICS

ODDS-RATIOS

...

CAN BE CONVERTED INTO COMMON UNIT

# MODELING

## FIXED VS RANDOM EFFECTS MODELS

FIXED EFFECT MA:

ASSUMES THAT TRUE EFFECT DOES NOT VARY BETWEEN STUDIES  
AND THAT VARIATIONS IN OBSERVED EFFECTS ARE DUE TO SAMPLING ERROR

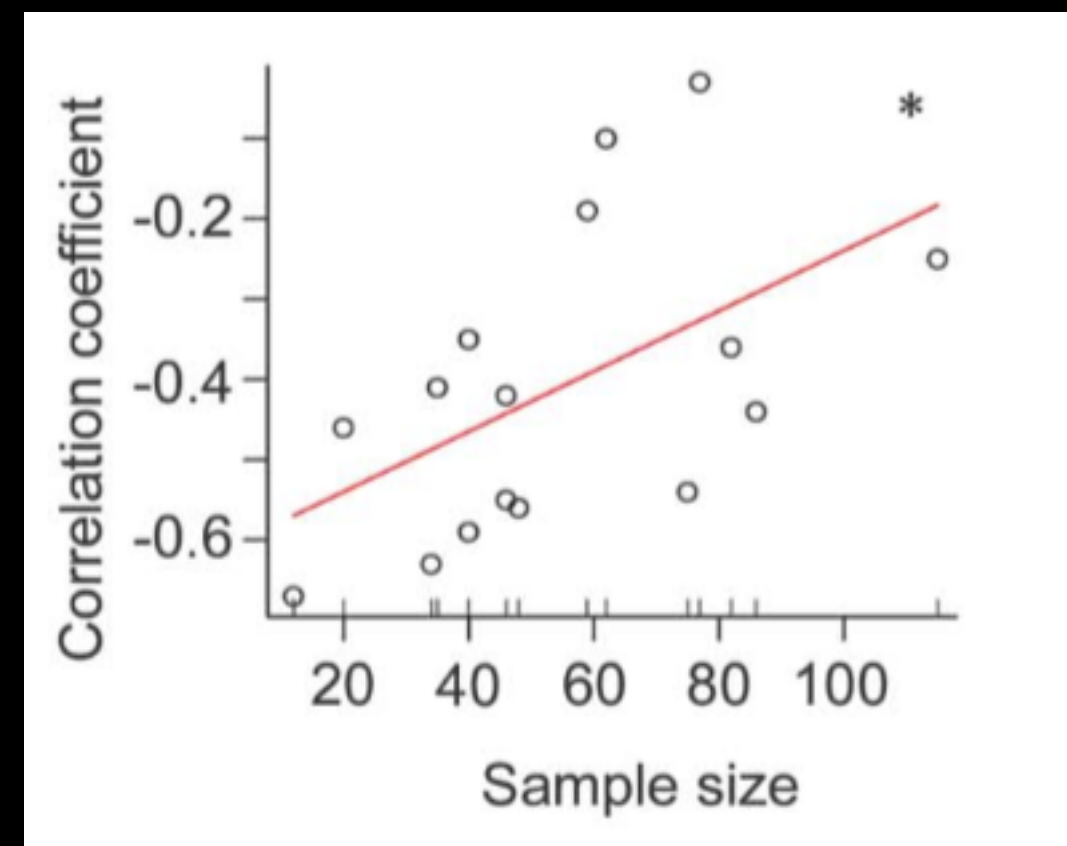
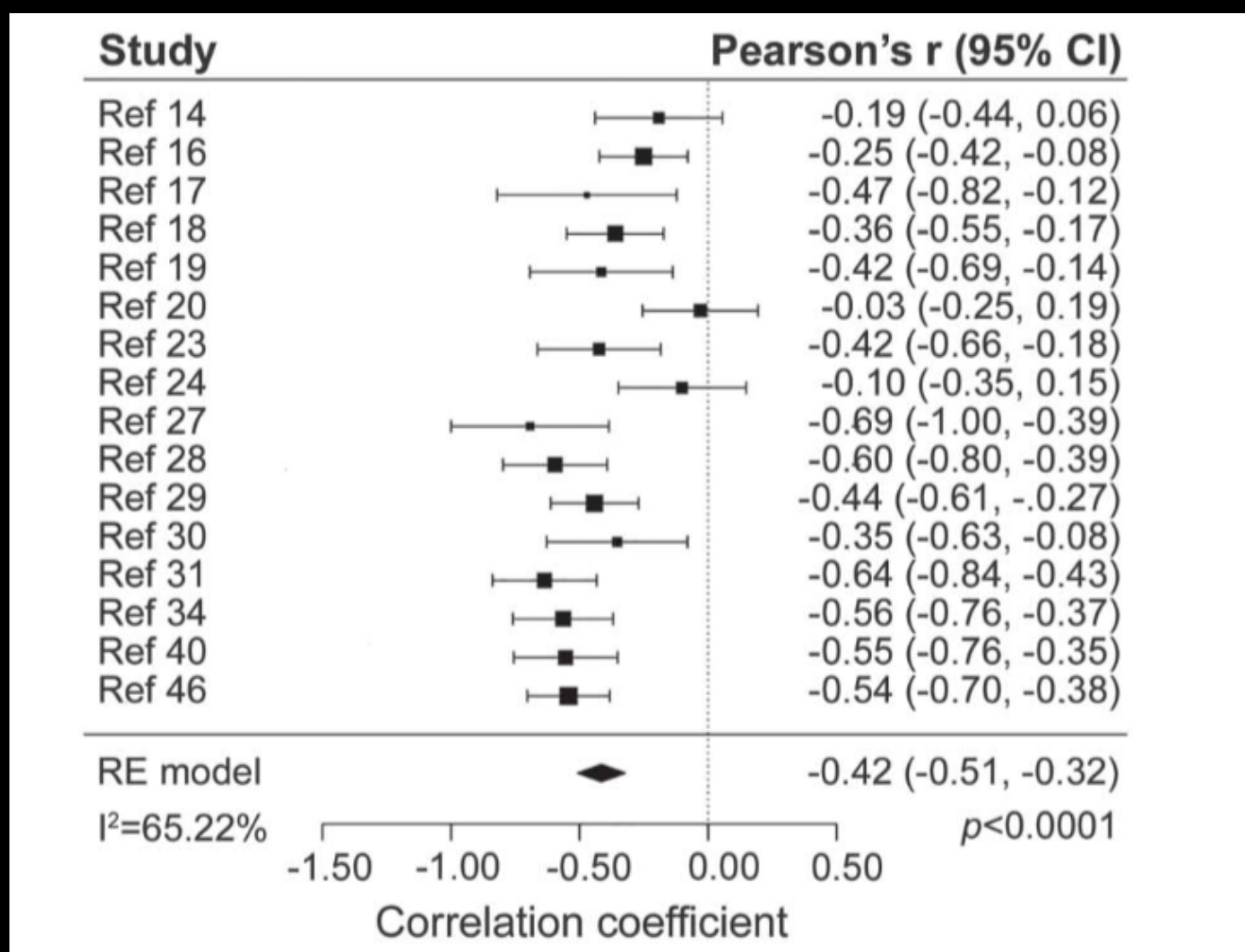
RANDOM EFFECTS MA:

ASSUMES THAT TRUE EFFECT DOES VARY BETWEEN STUDIES  
AND THAT VARIATION IN EFFECTS ARE DUE TO SAMPLING ERROR

RANDOM EFFECTS GENERALLY RECOMMENDED

# TOOLS

## METAFOR FOR R



# TOOLS

```
# load table
setwd(MYPATH)
db = read.table(MYDAT.csv,header=T,sep=',')
attach(db)

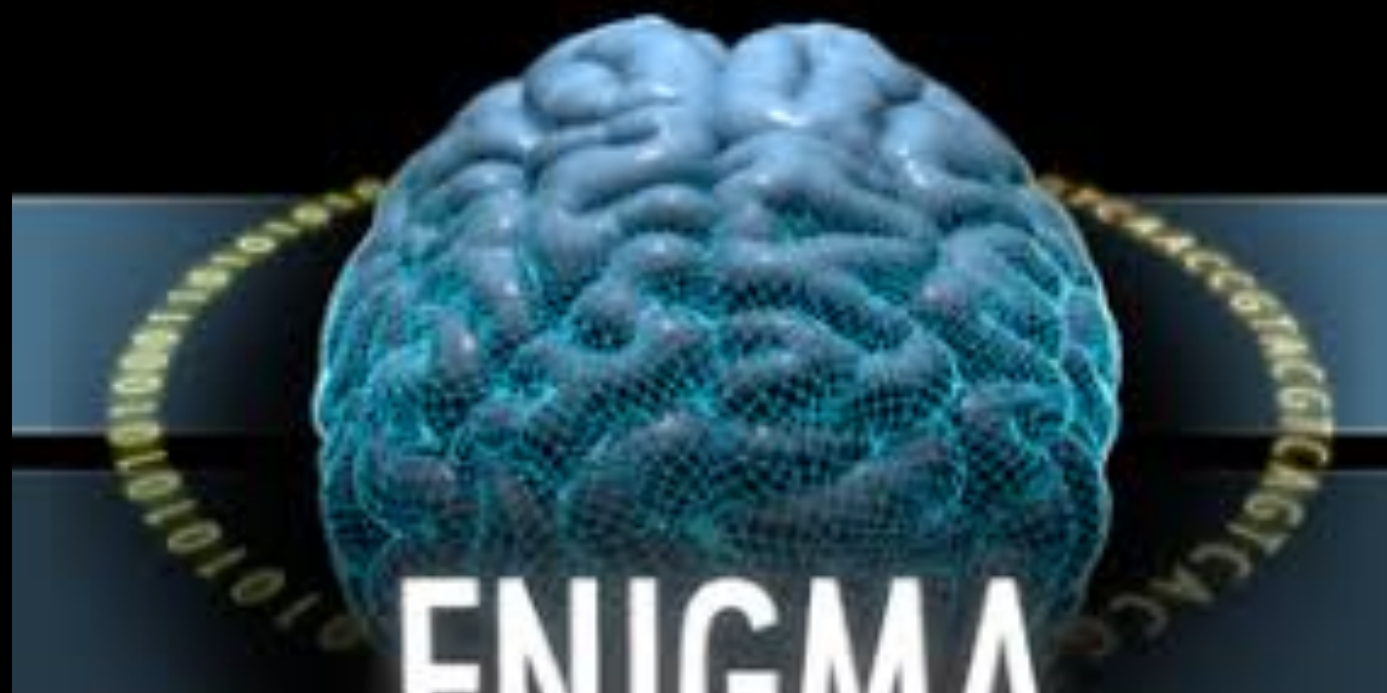
# variables
myVAR = factor(myvariable);
mySN = factor(mystudy);

dat = escalc(measure="UCOR", ri=EFFECT, ni=N, data=db)

# model
mod = rma.mv(yi, vi, data=dat, level=95, random=~1|mySN, method="REML")

summary(mod)
funnel.rma(mod)
forest.rma(mod)
```

ENIGMA



# ALE

brainmap.org

home taxonomy software tools publications collaborations credits contact

GingerALE Version 2.3.6

GingerALE is the BrainMap application that is used to perform an ALE meta-analysis on coordinates in Talairach or MNI space. GingerALE can also be used to convert coordinates between MNI and Talairach spaces using the [icbm2tal](#) transform.



The ALE meta-analysis method was initially developed by Peter Turkeltaub ([Turkeltaub et al., 2002](#)). This method of meta-analysis was adopted by BrainMap in 2003. Several modifications have been made to the ALE algorithm since then, and the current version of our software is reported in [Eickhoff et al., 2009](#).

All output files are written in [NIfTI \(.nii\)](#) format. The input for a meta-analysis can be a set of coordinates in Talairach or MNI space, or a set of

**Downloads (Updated 26.Apr.2016)**

-  Download Mac
-  Download PC
-  Download Other

**GingerALE Forum**

Have a question or comment?

- [brainmap.org/forum](#)

We love to hear from you!

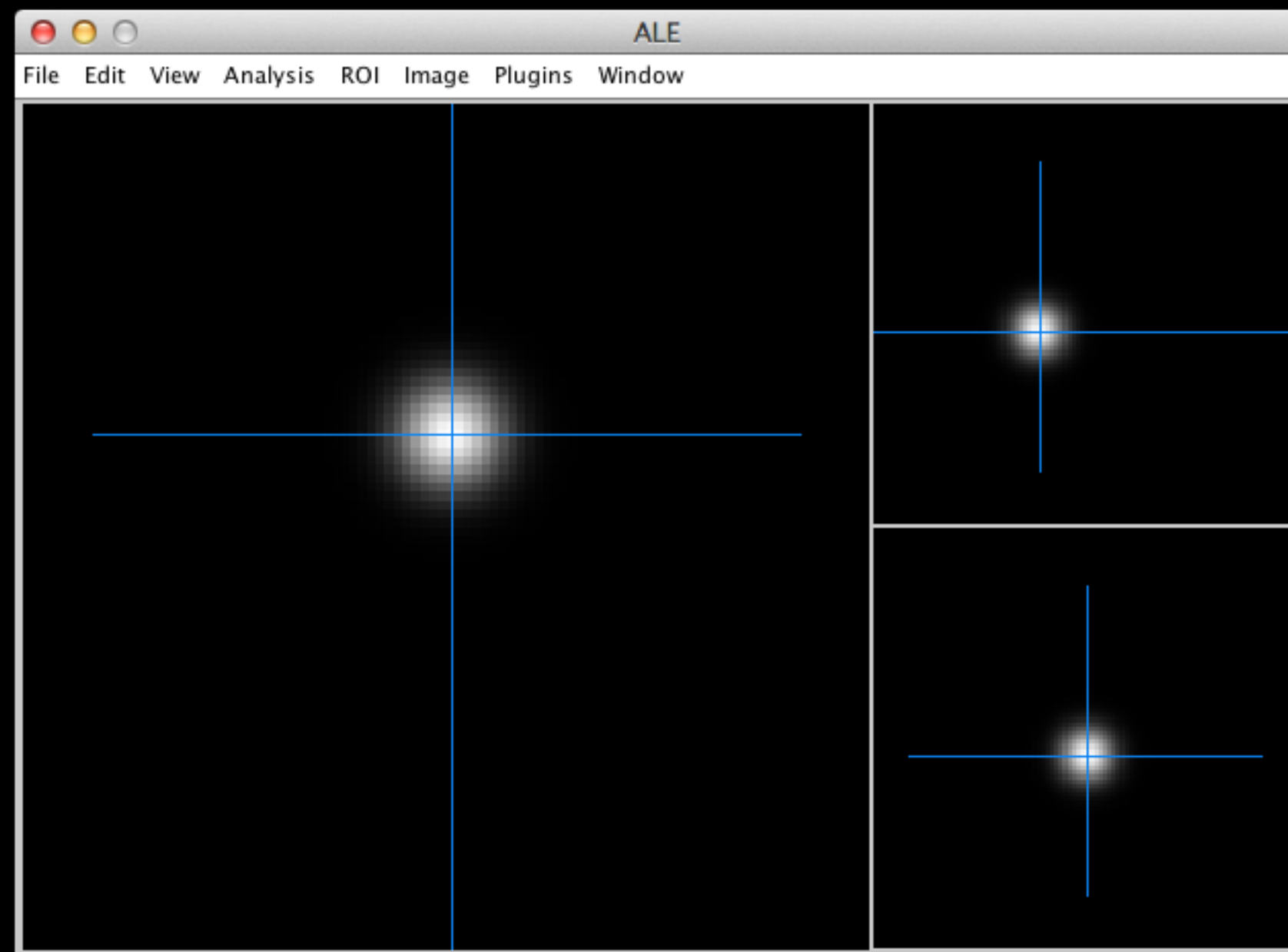
**Documentation**

-  GingerALE README
-  GingerALE License
-  GingerALE Users' Manual

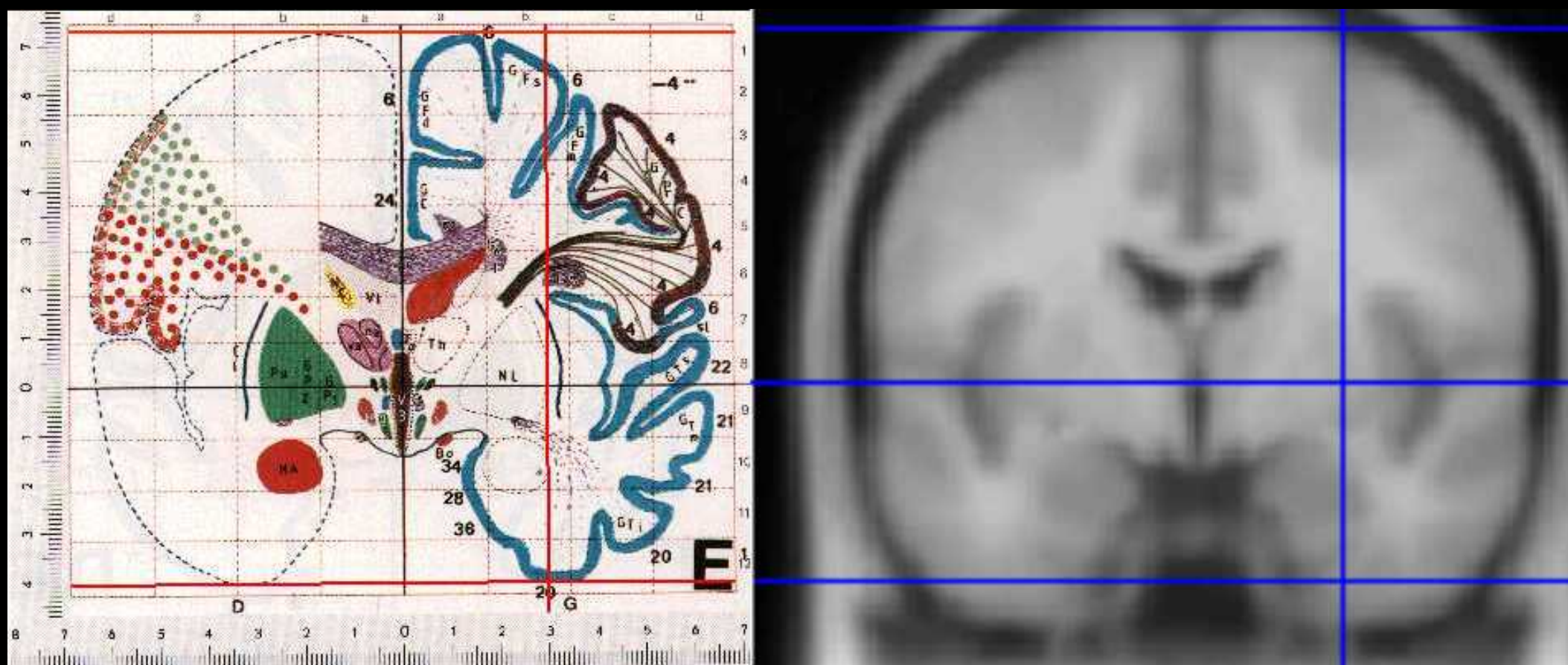
**Anatomical Template**

Once the thresholded ALE map has been created, you'll need an

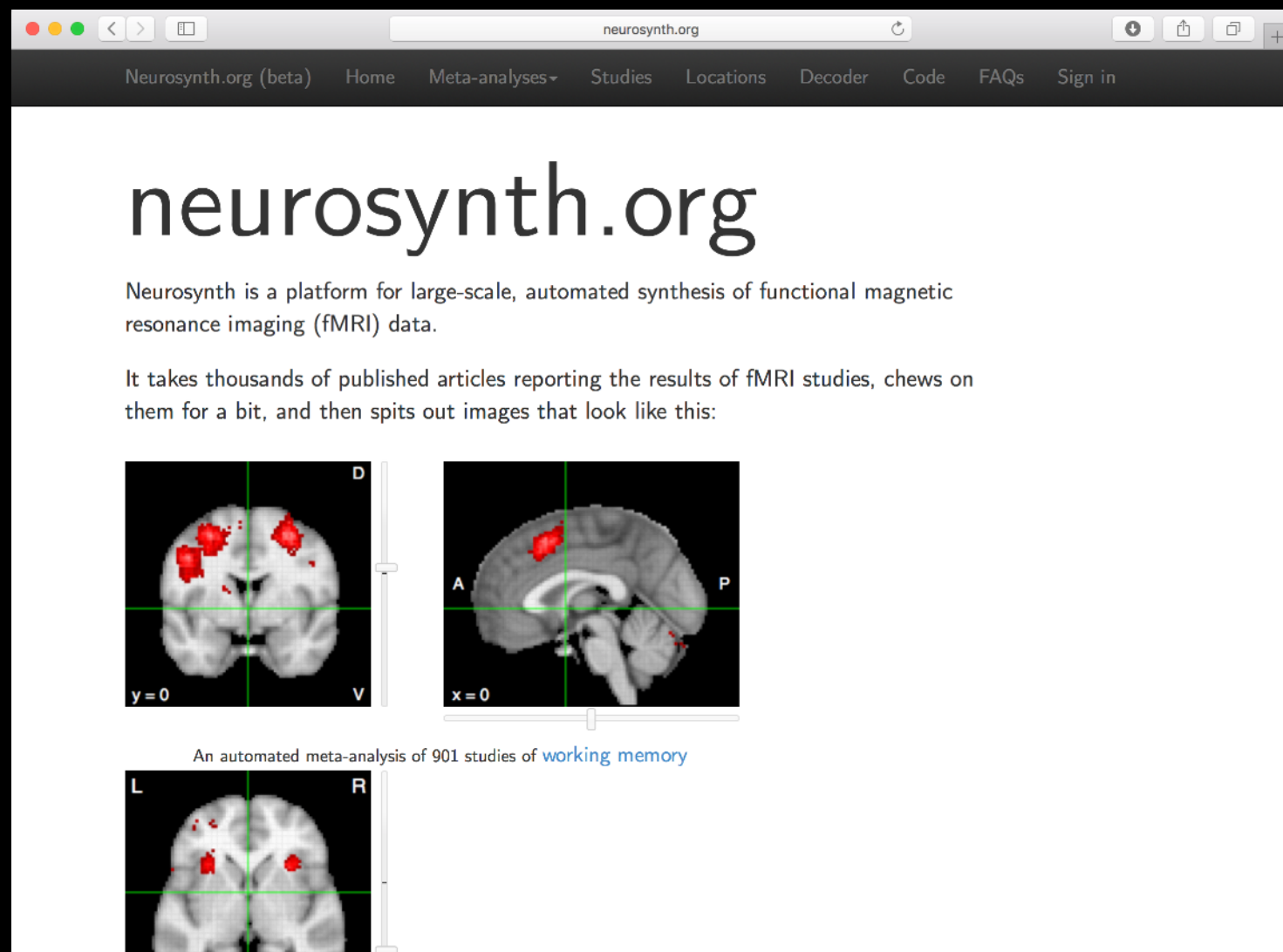
# ALE



ALE



# NEUROSYNTH



# NEUROSYNTH

## How are these images generated?

- Activation coordinates are extracted from published imaging articles using an automated parser.
  - The full text of all articles is parsed, and each article is 'tagged' with set of highh terms that occur at a high frequency in that article.
- A list of several thousand terms that occur at high frequency in 20 or more studies is generated.
  - For each term of interest (e.g., 'emotion', 'language', etc.), the database of coordinates is divided into two sets: those that occur in articles containing the term, and those that don't.
  - A giant meta-analysis is performed comparing the coordinates reported for studies with and without the term of interest.

In addition to producing statistical inference maps (i.e., z and p value maps), we also compute posterior probability maps, which display the likelihood of a given term being used in a study if activation is observed at a particular voxel.

# NEUROSYNTH

## Forward/reverse inference

- Forward inference map:

z-scores corresponding to the likelihood that a region will activate if study uses a particular term (i.e.,  $P(\text{Activation}|\text{Term})$ )

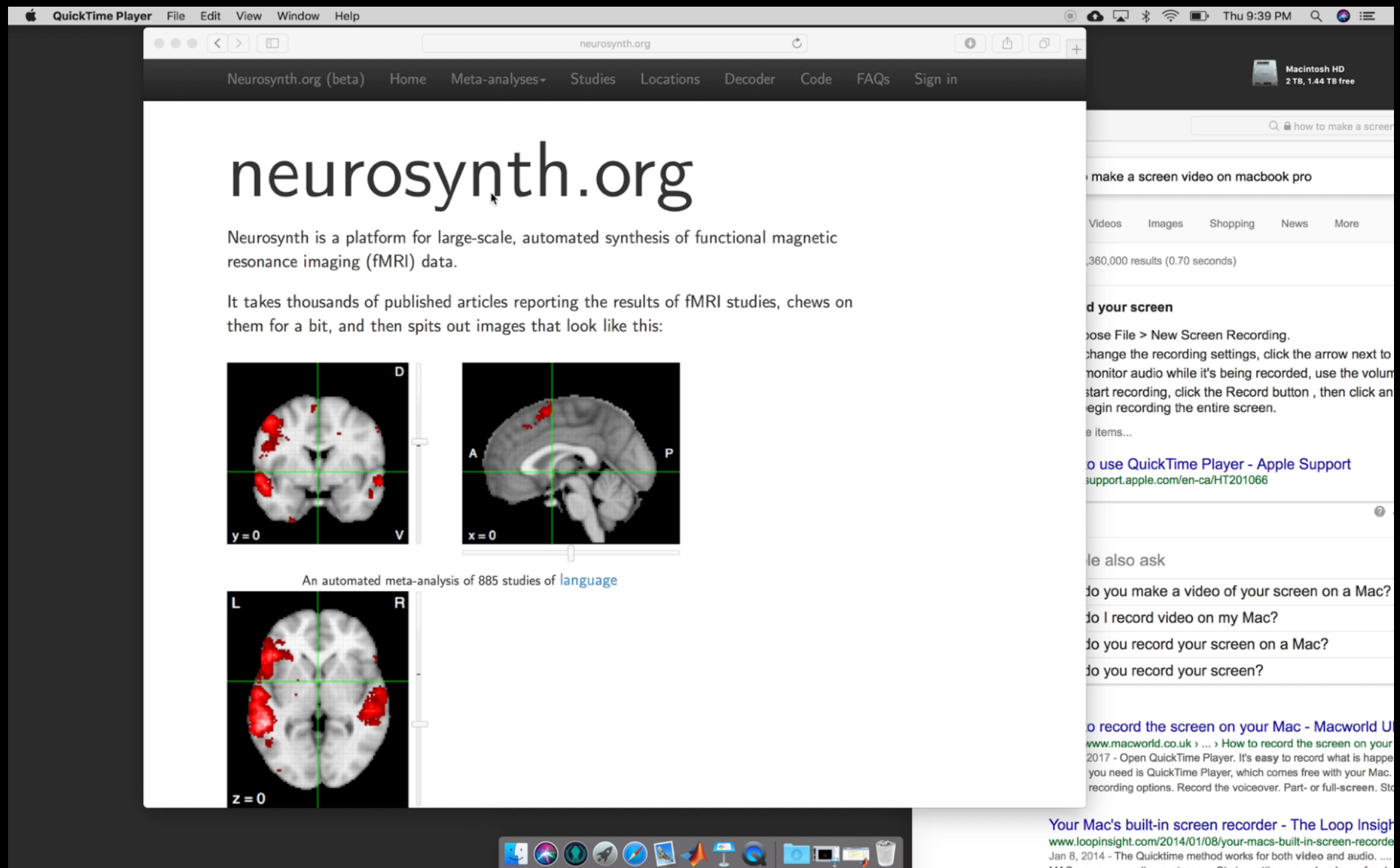
- Reverse inference map:

z-scores corresponding to likelihood that term is used in study given presence of reported activation (i.e.,  $P(\text{Term}|\text{Activation})$ )

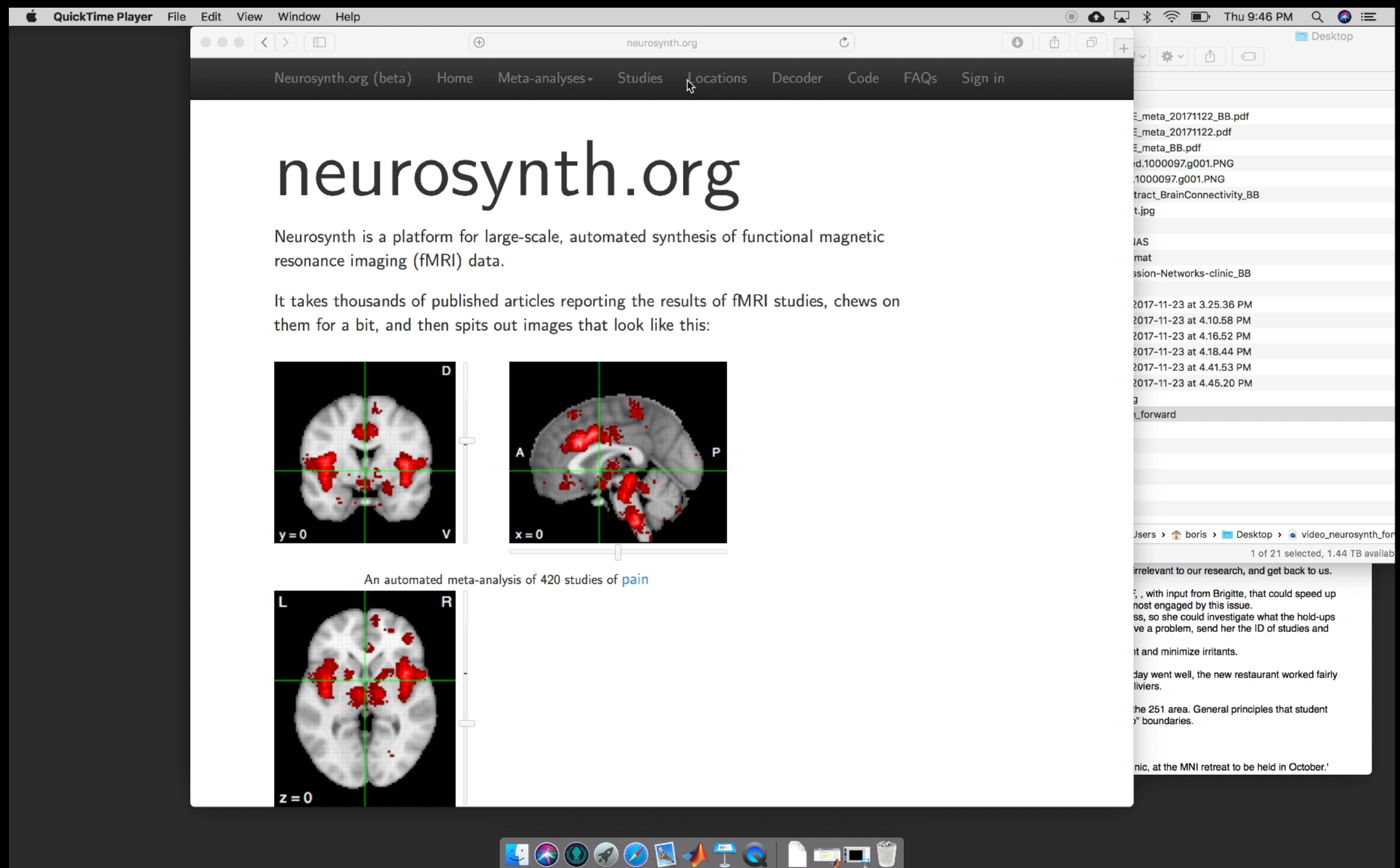
- Posterior probability map:

estimated probability of term used given presence of activation (i.e.,  $P(\text{Term}|\text{Activation})$ ).

# NEUROSYNTH



# MACM



# NEUROSYNTH

## Forward/reverse inference

- Forward inference map:

z-scores corresponding to the likelihood that a region will activate if study uses a particular term (i.e.,  $P(\text{Activation}|\text{Term})$ )

- Reverse inference map:

z-scores corresponding to likelihood that term is used in study given presence of reported activation (i.e.,  $P(\text{Term}|\text{Activation})$ )

- Posterior probability map:

estimated probability of term used given presence of activation (i.e.,  $P(\text{Term}|\text{Activation})$ ).

# #cingulategate



## The dorsal anterior cingulate cortex is selective for pain: Results from large-scale reverse inference

Matthew D. Lieberman<sup>1</sup> and Naomi I. Eisenberger

Department of Psychology, University of California, Los Angeles, CA 90095-1563

Edited by Richard Ivry, University of California, Berkeley, CA, and accepted by the Editorial Board October 26, 2015 (received for review July 30, 2015)

Dorsal anterior cingulate cortex (dACC) activation is commonly observed in studies of pain, executive control, conflict monitoring, and salience processing, making it difficult to interpret the dACC's specific psychological function. Using Neurosynth, an automated brainmapping database [of over 10,000 functional MRI (fMRI) studies], we performed quantitative reverse inference analyses to explore the best general psychological account of the dACC function  $P(\Psi \text{ process} | \text{dACC activity})$ . Results clearly indicated that the best psychological description of dACC function was related to pain processing—not executive, conflict, or salience processing. We conclude by considering that physical pain may be an instance of a broader class of survival-relevant goals monitored by the dACC, in contrast to more arbitrary temporary goals, which may be monitored by the supplementary motor area.

dACC | pain | reverse inference | Neurosynth

Of all the regions in the brain that have received heavy study

And while I'll be the first to admit that I know very little about the anterior cingulate cortex, I am probably the world's foremost expert on Neurosynth\*—because I created it.

I also have an obvious interest in making sure that Neurosynth is used with appropriate care and caution.

In what follows, I provide my HIBAR reactions to the Lieberman & Eisenberger (2015) manuscript, focusing largely on whether L&E's bold conclusion is supported by the Neurosynth findings they review (spoiler alert: no).

LETTER

The field of human neuroimaging has taken a particular shine to the ACC in the past two decades; if you've ever heard overheard some nerdy-looking people talking about "conflict monitoring", "error detection", or "reinforcement learning" in the human brain, there's a reasonable chance they were talking at least partly about the role of the ACC.



LETTER

## Pain in the ACC?

Tor D. Wager<sup>a,b,1</sup>, Lauren Y. Atlas<sup>c,d</sup>, Matthew M. Botvinick<sup>e</sup>, Luke J. Chang<sup>f</sup>, Robert C. Coghill<sup>g</sup>, Karen Deborah Davis<sup>h,i,j</sup>, Gian Domenico Iannetti<sup>k</sup>, Russell A. Poldrack<sup>l</sup>, Alexander J. Shackman<sup>m,n,o</sup>, and Tal Yarkoni<sup>p</sup>

Lieberman and Eisenberger (1) claim that the "dorsal anterior cingulate cortex (dACC) is selective for pain." This surprising conclusion contradicts a large body of evidence showing robust dACC responses to nonpainful conditions. Electrophysiological and optogenetic studies have identified neuronal populations activated during foraging behavior, attention, emotion, reward expectancy, skeleto-motor and visceromotor activity, and other functions (e.g., refs. 2–5). Only a small minority of dACC neurons are pain-related.

Lieberman and Eisenberger (1) later propose that the dACC responds to "enduring survival-relevant goals," including hunger and social rejection. This hypothesis appears inconsistent with selectivity for pain, with attention- (3) and motor-coding (4) dACC neurons, and with demonstrations of dissociable representations of pain and rejection in dACC (6). We agree that dACC subserves survival-relevant functions; however, acceptance of dACC as "pain-selective" will lead the field down the wrong track.

Lieberman and Eisenberger's (1) conclusions are based on Neurosynth.org (7), a database of activation coordinates and words used in >11,000 neuroimaging studies. The claim of pain selectivity is based on a statistical preference

PAULI

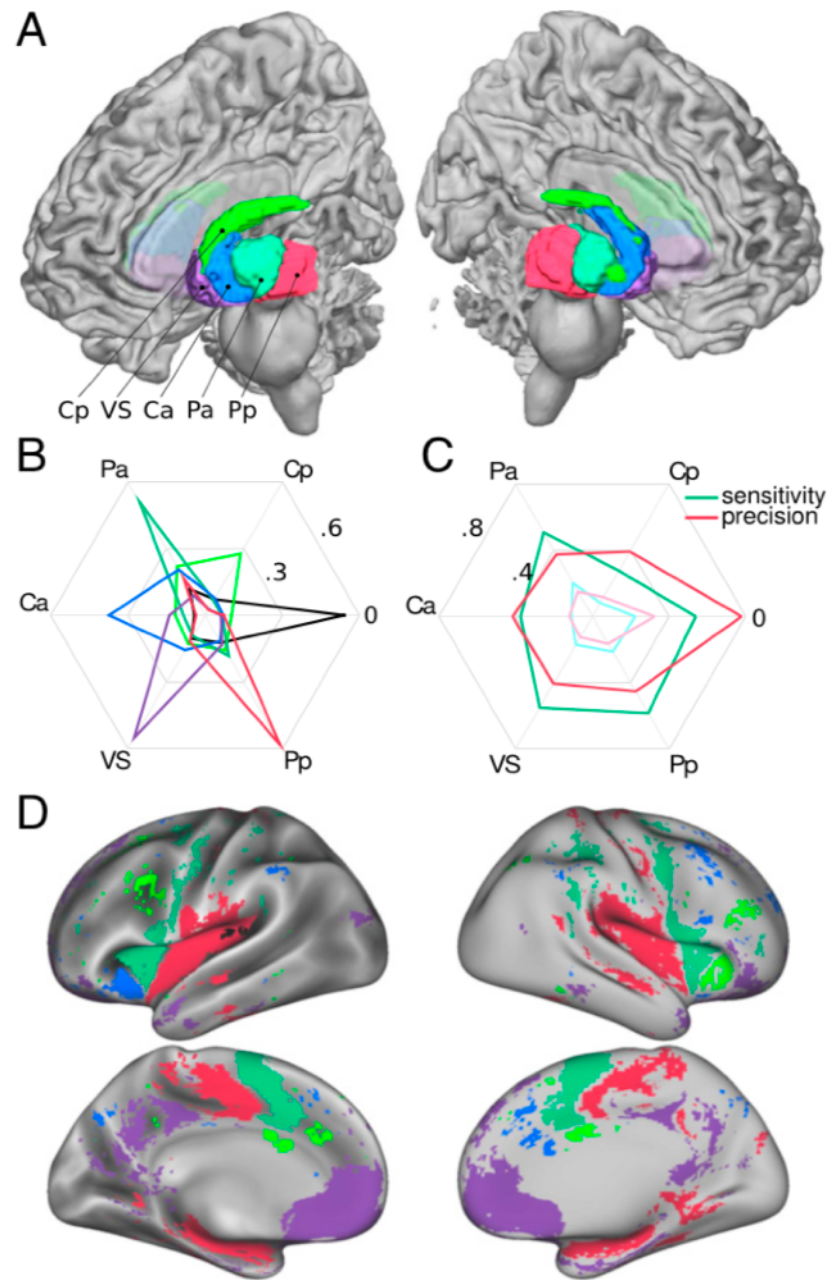


**Fig. 1.** (A) Cluster analysis ( $k$ -means,  $k = 5$ ) of corticostriatal coactivation patterns across imaging studies identified distinct striatal zones. The five zones showed strong bilateral symmetry. Symmetry analysis is shown in *SI Appendix, Fig. S3*, and results with different values of  $k$  are shown in *SI Appendix, Fig. S4*. (B) Based on the pattern of reported cortical activation, a naive Bayes classifier predicted which striatal zone was the most active one. The confusion matrix, shown as a polar plot, indicates the probability that the classifier predicted activation in the correct zone and the probability that it incorrectly predicted activation in one of the other zones. Category “0” represents studies with no striatal activation (i.e., no active zone). (C) Sensitivity (dark green) and precision (i.e., positive predictive value, dark red) of the classifier for each functional zone. Attenuated colors (light green and red) indicate chance performance levels in the permutation test. Actual performance exceeded chance levels substantially for each category. (D) Maximum a posteriori estimates from the naive Bayes classifier indicate which striatal zone is most strongly coactivated with each cortical voxel ( $q < 0.05$ , false discovery rate-corrected).

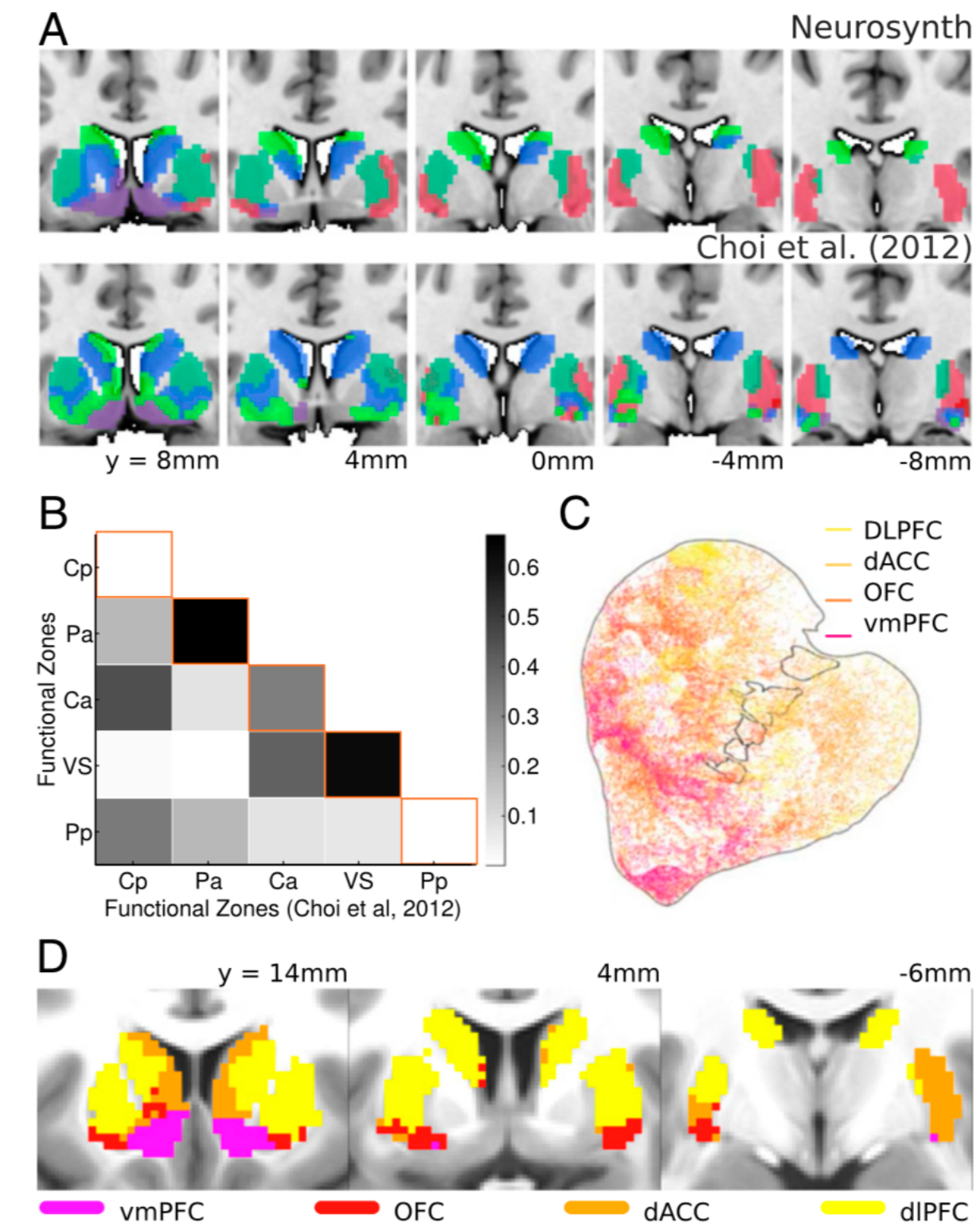


**Fig. 2.** (A) Side-by-side comparison of our parcellation with an existing  $k = 7$  striatal parcellation (17), based on RSFC, indicates that the two approaches only lead to moderately overlapping results. (B) Dice's coefficients of a zone-by-zone comparison of our results with the existing solution. (C) Recent anterograde tracer study in nonhuman primates found strong evidence for a gradient of frontal cortical-striatal axon projections (26). dIPFC, dorsolateral PFC. (D) Analysis of coactivation of each striatal voxel with the different regions of interest in C, defined here based on the AAL atlas (61), show a similar pattern in humans. Reprinted from ref. 26.

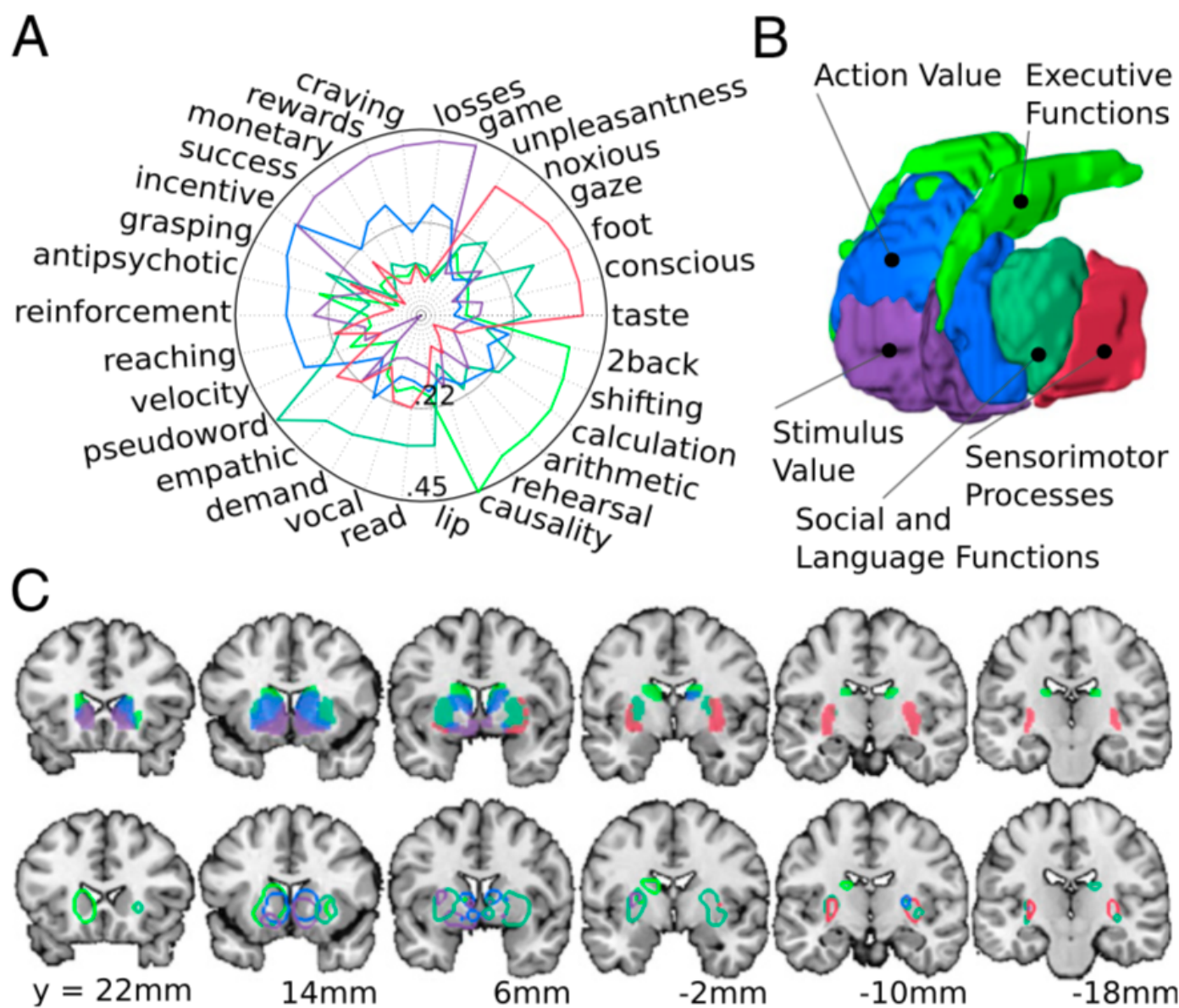


**Fig. 3.** To identify the psychological functions associated with each striatal zone, we calculated for each psychological term included in the NeuroSynth database its likelihood ratio of appearing in a study, given that activation was reported anywhere within a zone. (A) Distribution of likelihood ratios across functional zones indicates a clear functional dissociation. (B) Subjective summary of the main psychological function of each functional zone in a working model. (C) Based on the reported striatal activation and the occurrence of psychological terms in each study, it was possible to identify the most representative studies for each functional zone. The striatal zones identified in our coactivation analysis (*Top*) and a reconstructed outline of the activation reported in the representative studies (*Bottom*) are shown.

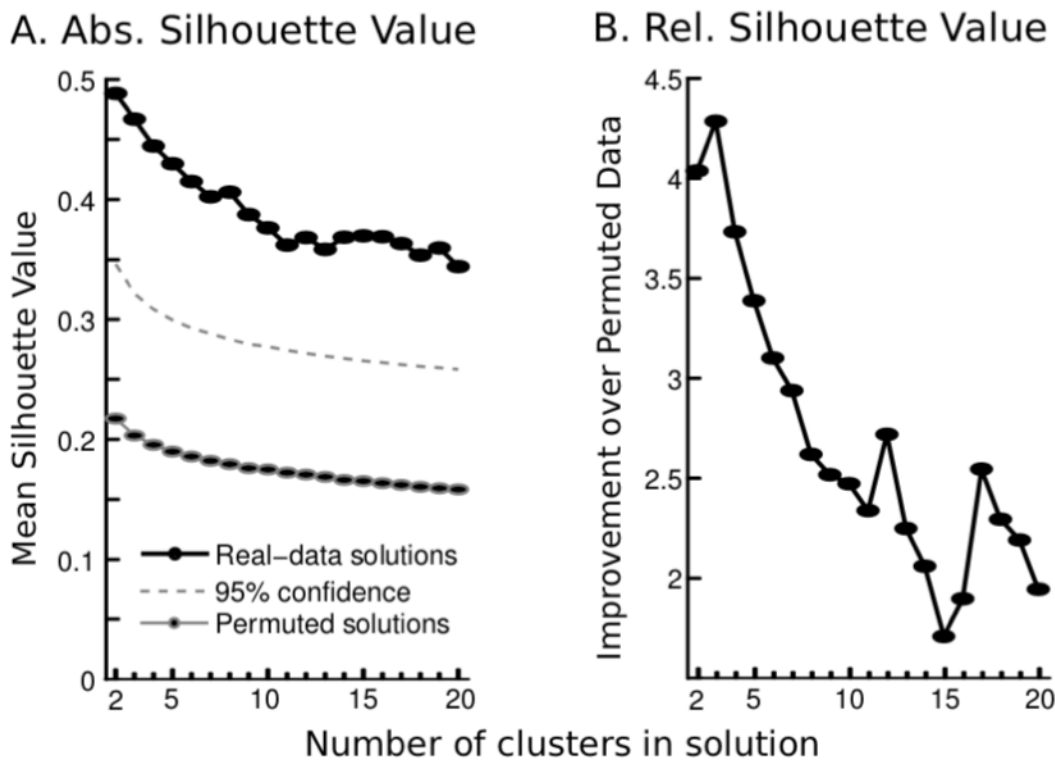


**Fig. S1.** In terms of cluster quality, none of the 19 cluster solutions ( $k=2-20$ ) emerged as a clear winner, but all solutions were clearly better than chance. To assess cluster quality, we used Monte-Carlo simulations to establish statistical significance against a null hypothesis that the clusters are randomly distributed across striatal voxels. For this purpose the columns in the striatal voxel (rows) by cortical voxel (columns) correlation matrix were permuted, k-means was run on that permuted correlation matrix, and the silhouette value was calculated [8]. We used a minimum of 134 permutations for each cluster solution, and found that this resulted in a very stable estimate of cluster quality.

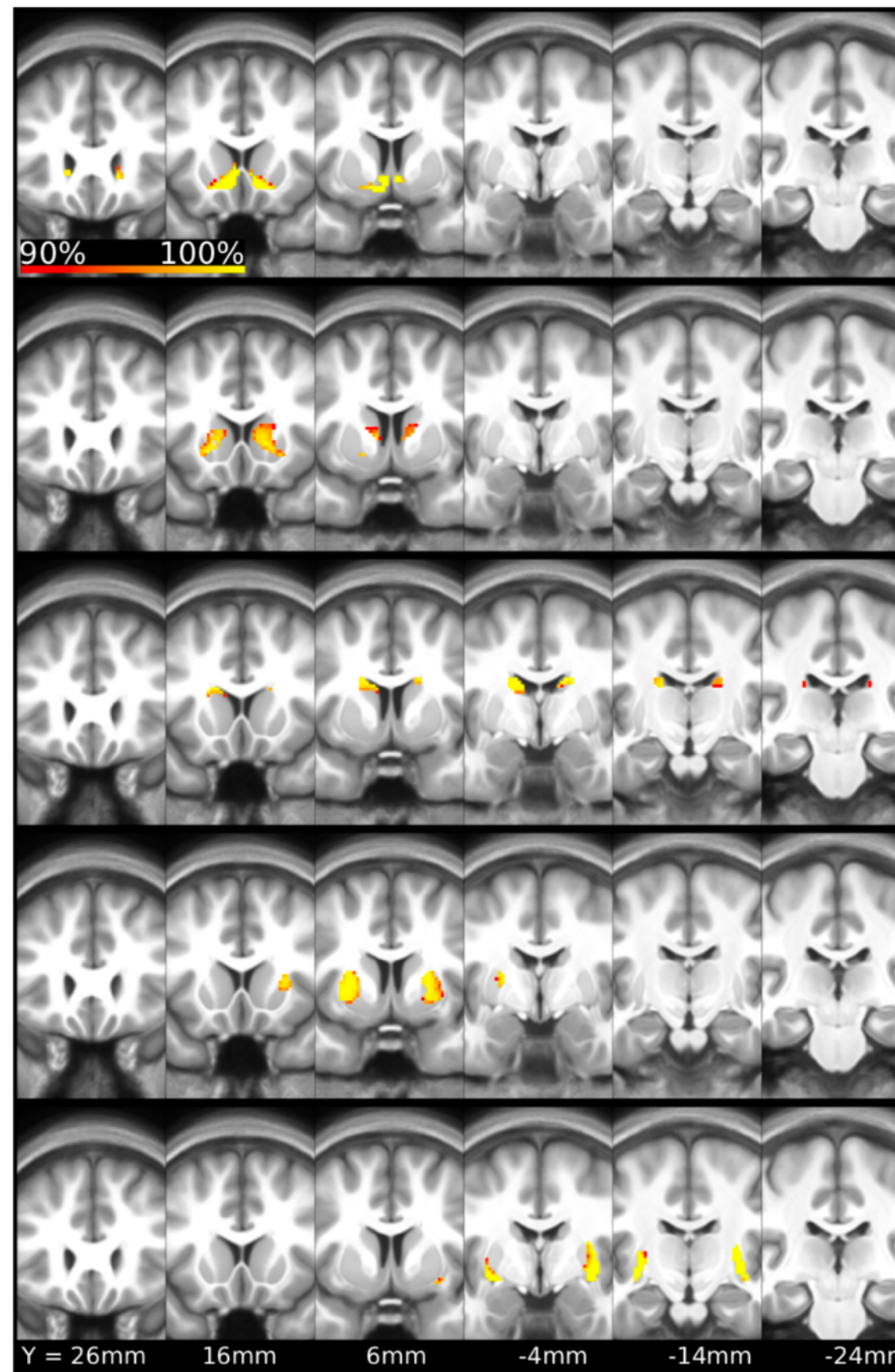


**Fig. S2.** Probabilistic maps of our five-cluster solution. Probabilistic maps were created by drawing 1000 bootstrap samples of the studies included in the database. Probabilities reflect the likelihood that a voxel was assigned to the same striatal zone across bootstrap samples (see Supplementary Information “Naïve Bayes classifier”). For example, if a voxel was assigned to the same striatal zone by the cluster analysis (after clusters were matched across bootstrap samples using nearest-neighbor similarity assessed by Dice’s coefficient) in 998 of the 1000 bootstrap samples, this would yield a probability of 99.8%. The average Dice coefficient between these 1000 solutions and the solution reported in the manuscript was 0.89 ( $SD=0.048$ ).

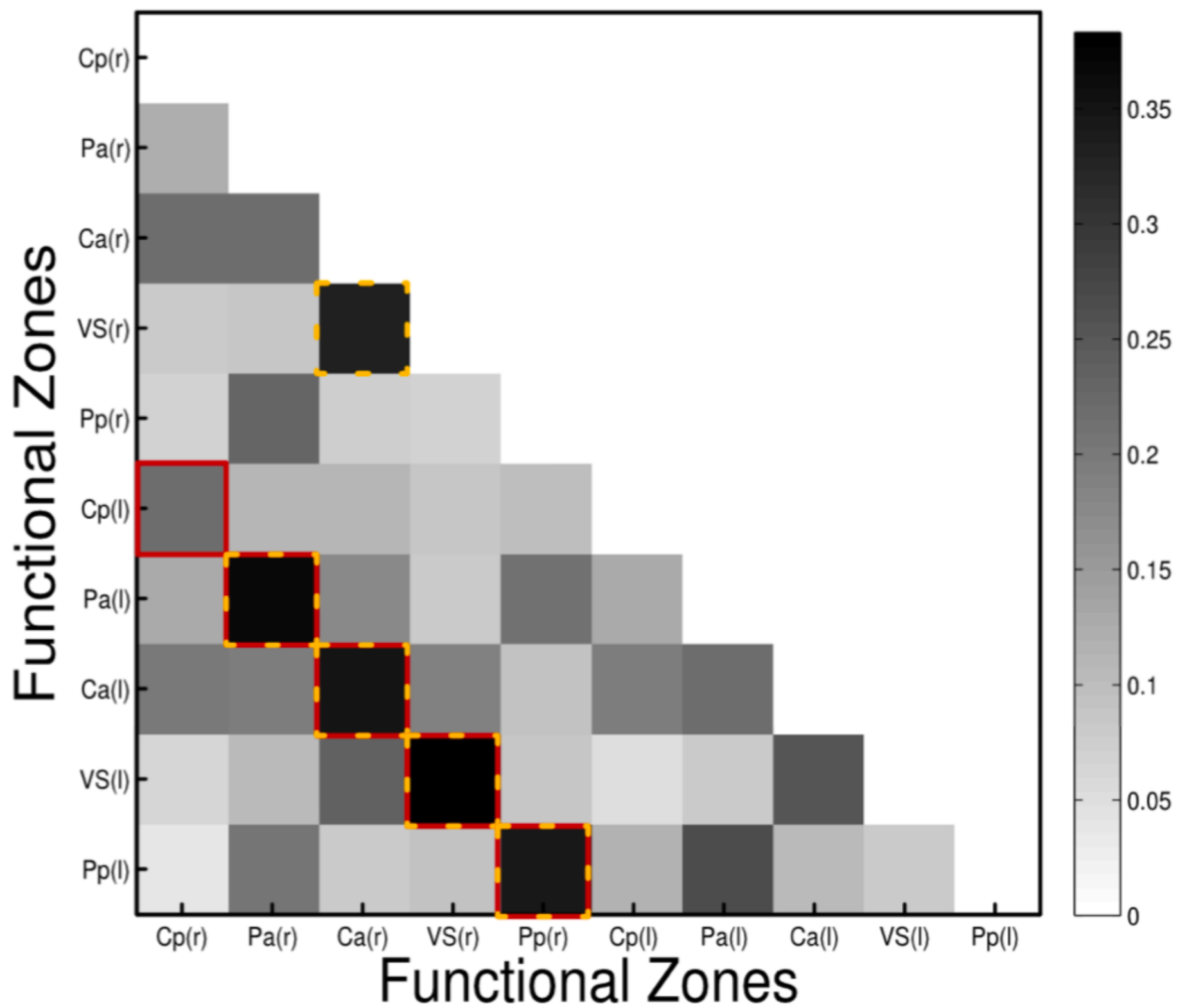


**Fig. S3.** To evaluate hemispheric symmetry of each functional zone, we evaluated for each zone how strongly its activation (proportion of active voxels within zone) in one hemisphere correlated with the same zone in the opposite hemisphere, and with all other zones in the same and opposite hemisphere.

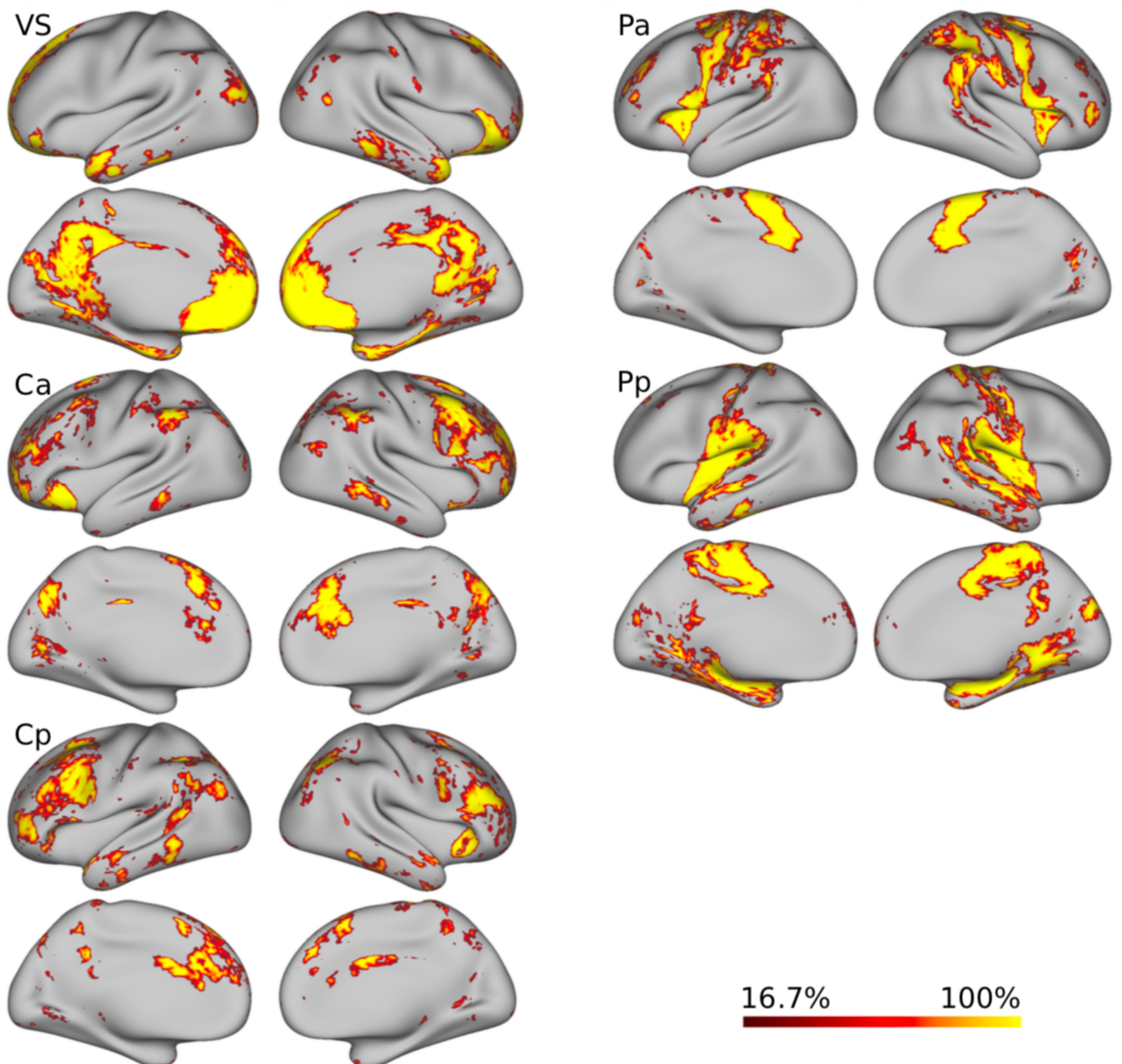


**Fig. S5.** Maximum a posteriori (MAP) estimates of how reliably a cortical voxel was co-activated with the different functional zones. MAP estimates were determined by drawing 1000 bootstrap samples from the studies included in the database, and training a naïve Bayes classifier to predict which striatal is reported to be the most active in each study, based on the pattern of reported cortical activation. In a final step, we counted for each voxel, how often it would be more strongly associated with one striatal zone, than with any other striatal zone.

CROSSLEY

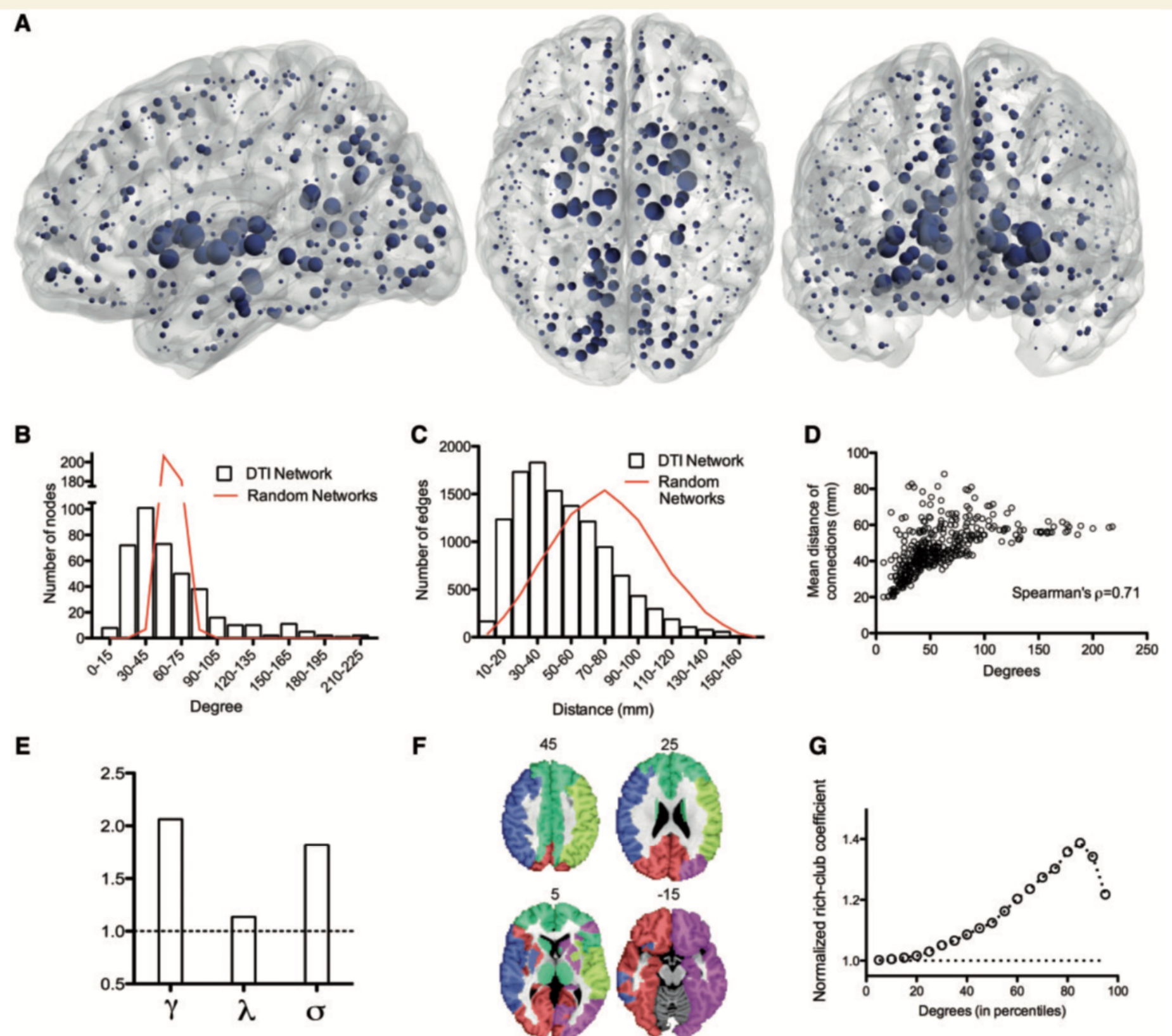


**Figure 1** Topological characteristics of the normal brain anatomical network (DTI connectome). **(A)** Nodes of the normal DTI network in anatomical space; the size of each node is proportional to its degree. **(B)** Fat-tailed degree distribution of DTI network (histogram) indicating higher probability of hubs than in a random (Erdős-Rényi) graph (red line). **(C)** Distance distribution of DTI networks (histogram) and of random graphs matched for degree distribution (red line). **(D)** Scatterplot of degree versus mean connection distance in the DTI network. **(E)** Small-world properties of the network ( $\gamma$  = normalized clustering coefficient;  $\lambda$  = normalized path length;  $\sigma$  = ratio of  $\gamma$  to  $\lambda$ ; dotted line = 1, the expected value of all these metrics in a random graph). **(F)** Modular decomposition of the DTI network. **(G)** Plot of the normalized rich club coefficient (y-axis) as a function of degree threshold (x-axis) used to define the rich club; dotted line = 1, the expected value of the normalized rich-club coefficient in a random network with the same degree distribution as the DTI connectome.

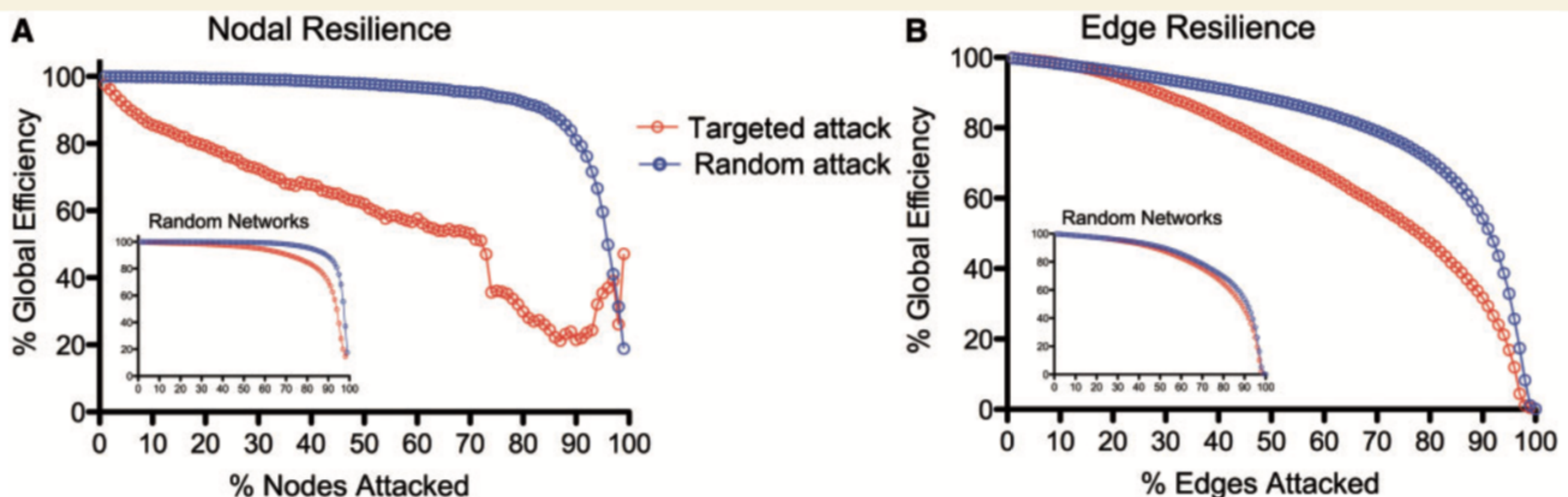


**Figure 2** Computational attacks and the resilience of the DTI connectome. **(A)** Plot of global efficiency of the DTI network versus percentage of nodes deleted. When nodes are deleted randomly the efficiency of the network is approximately as resilient as a random (Erdős-Rényi) graph (*inset*); when high degree nodes are targeted (deleted in order of decreasing degree) the efficiency of the network degrades more rapidly than a random graph. **(B)** Plot of global efficiency of the DTI network versus percentage of edges deleted. The efficiency of the DTI network degrades faster than a random graph when the longer distance edges are targeted (deleted in order of decreasing connection distance).

**Table 1** Disorders included in the meta-analysis of grey matter lesions based on previously published voxel-based morphometry (VBM) studies

Disorder	Number of VBM studies included	Number of patients	Number of healthy controls
Attention deficit hyperactivity disorder	13	363	331
Amyotrophic lateral sclerosis	8	132	146
Anorexia nervosa	10	156	207
Asperger's syndrome	9	163	209
Autism (pervasive developmental disorder excluding Asperger's syndrome)	12	330	331
Bipolar affective disorder	18	479	630
Chronic pain	13	305	326
Dementia in Alzheimer's disease	36	765	1211
Dementia in Parkinson's disease	10	192	228
Depressive disorder	24	883	1015
Developmental dyslexia	8	121	122
Dystonia	10	219	244
Frontotemporal dementia	37	508	660
Hereditary ataxia	15	202	223
Huntington's disease	9	227	193
Juvenile myoclonic epilepsy	7	220	218
Multiple sclerosis	11	499	353
Obsessive-compulsive disorder	14	425	431
Obstructive sleep apnoea	7	177	268
Panic disorder	7	142	133
Parkinson's disease	17	515	411
Progressive supranuclear palsy	7	108	182
Post traumatic stress disorder	14	232	327
Schizophrenia	51	1925	2133
Temporal lobe epilepsy – left	14	339	597
Temporal lobe epilepsy – right	10	247	373
Total	392	9874	11 502

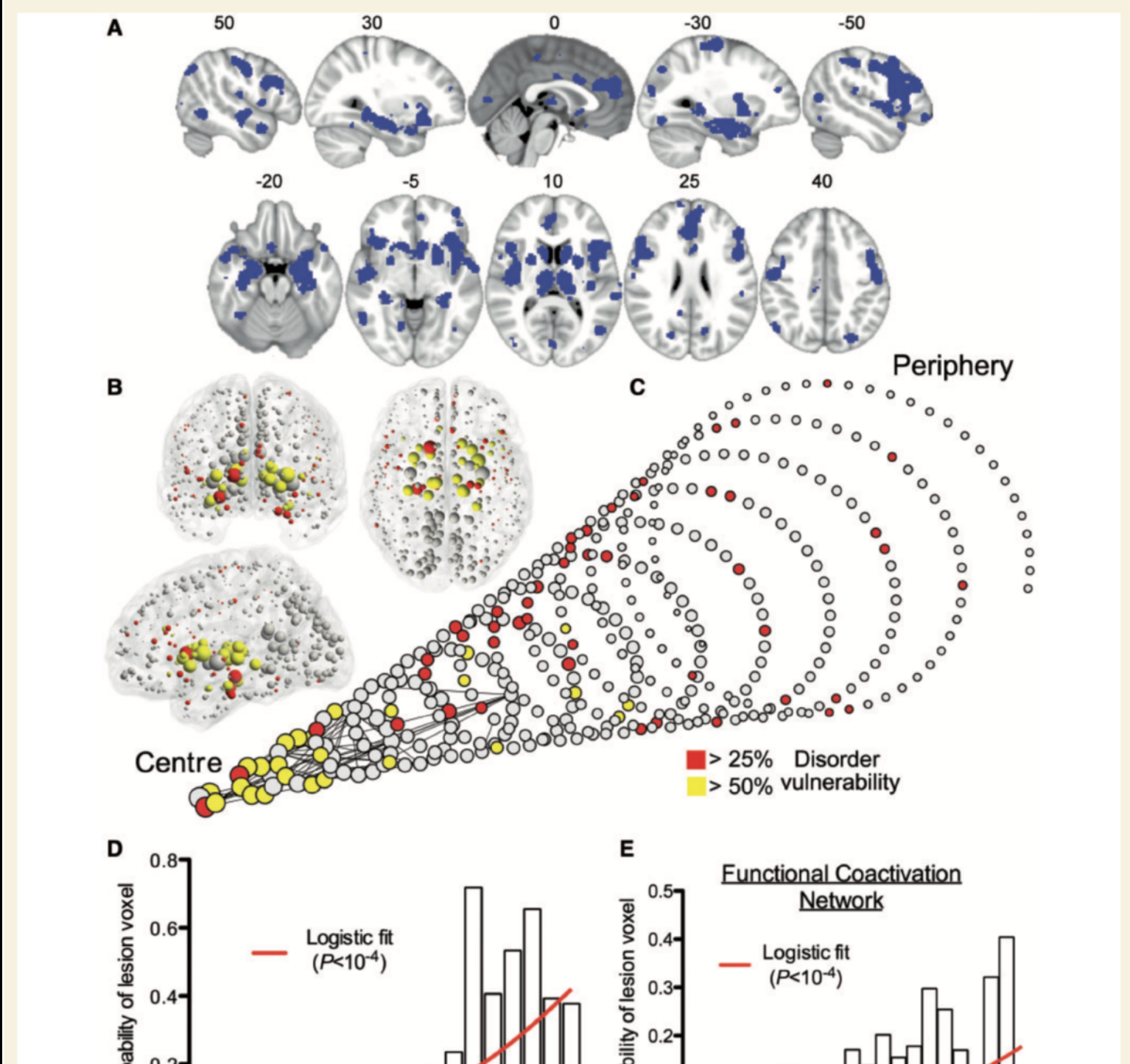


**Figure 3** MRI lesions identified meta-analytically from the primary literature on 26 clinical brain disorders impact preferentially on the hubs of the normal connectome. **(A)** A meta-analytic map of multiple cortical and subcortical grey matter MRI lesions that were significantly abnormal ‘on average’ over 26 specific disorders. **(B)** Nodes of the normative DTI connectome, represented in anatomical space, and **(C)** in a spiral, where nodes of similar degree are arranged in the same circle, and the different circumferences arranged so that the tip of the spiral has the highest degree hub nodes, while the base the most peripheral nodes. Nodes are sized in proportion to their degree, and coloured according to the proportion of voxels which are generically lesioned, i.e. the percentage of lesion voxels each node comprises. The strongest 0.1% of edges between nodes, which highlight pairs of nodes with consistently high number of streamlines interconnecting them, are shown for illustrative purposes. **(D)** Plot of the probability of lesion voxels (y-axis) versus the degree of DTI connectome nodes (x-axis). The red line is a fitted logistic regression model. **(E)** Plot of the probability of lesion voxels (y-axis) versus the degree of the functional co-activation network nodes (x-axis). The red line is a fitted logistic regression model.

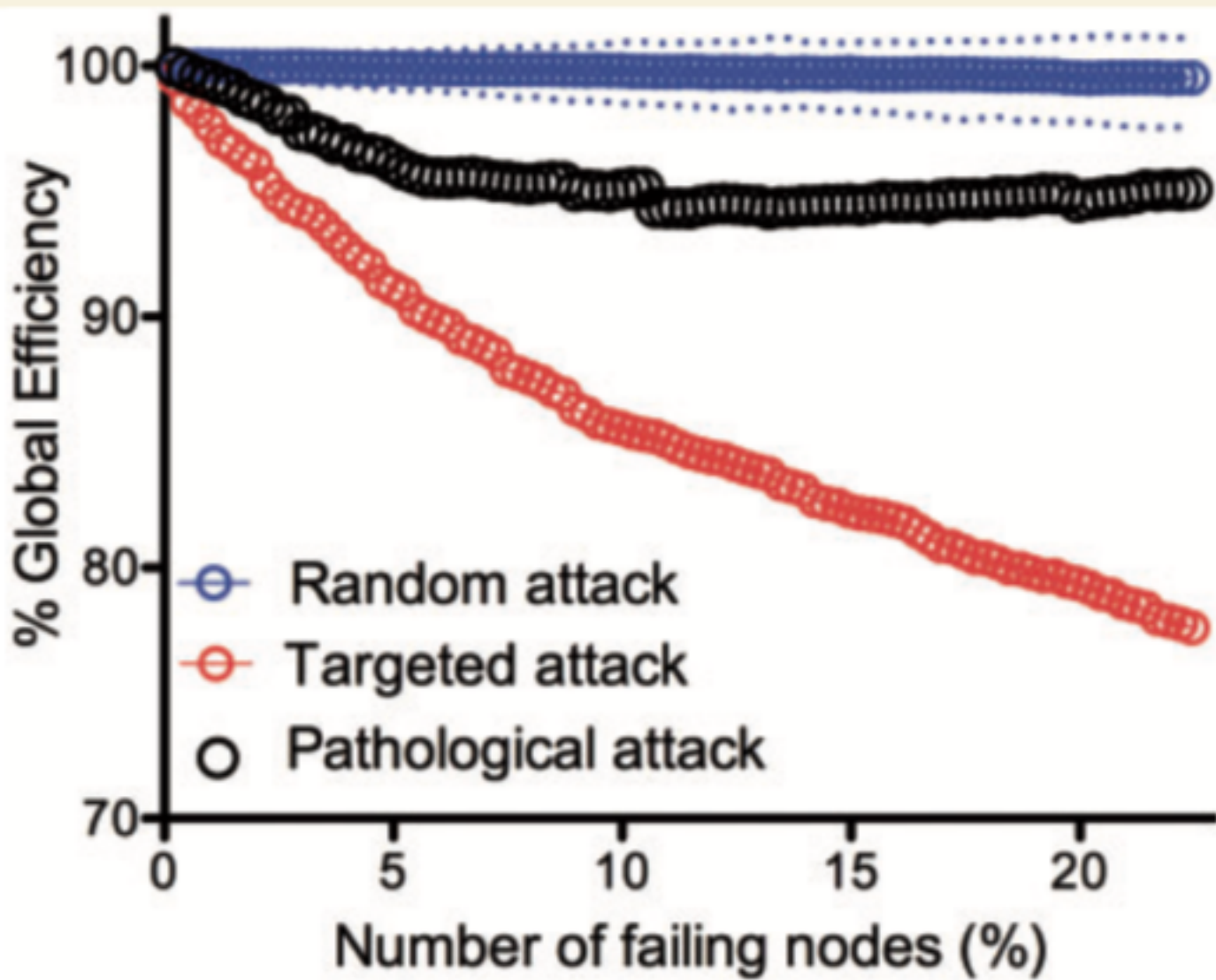


**Figure 4** Modelling pathological attack on the connectome.  
Plot of the global efficiency of the DTI network versus percentage of nodes deleted. Note that the global efficiency deteriorates significantly faster in pathological attacks compared to random attack, but not to the extent of targeted attacks on hubs.

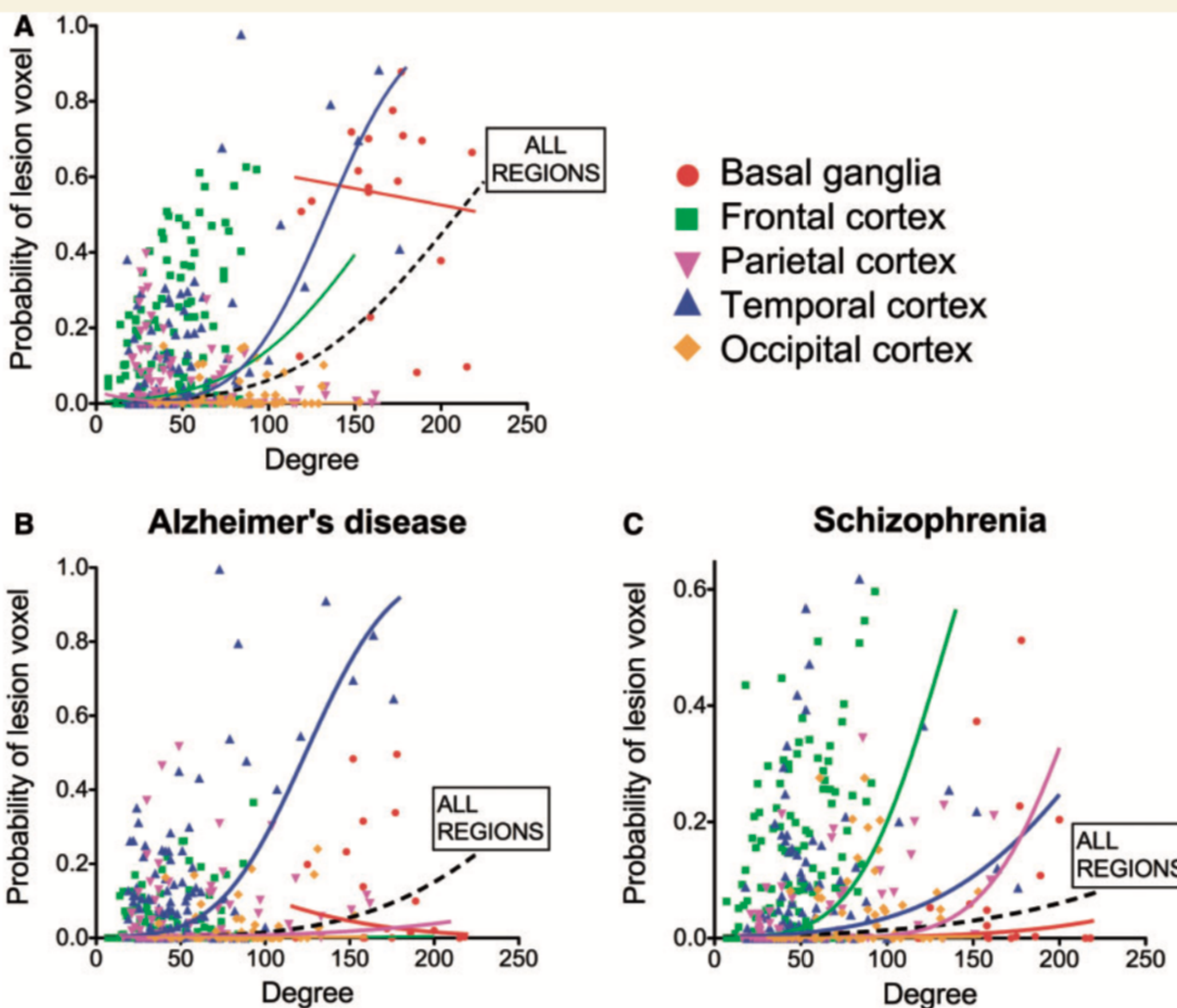


**Figure 5** Degree and probability of lesion in anatomical subnetworks. Probability of a 'voxel lesion' in each of the 401 regions of the DTI template for (A) the disorder-general VBM meta-analysis, as well as for (B) Alzheimer's disease and (C) schizophrenia meta-analysis. Nodes have been colour-coded according to their anatomical (lobar) location, and logistic regression lines for each subgroup and for all the regions together are shown.

# Brain Disorders

Amyotrophic lateral sclerosis  
Dystonia  
Developmental dyslexia  
Anorexia nervosa  
Obsessive-compulsive disorder  
Parkinson's disease  
Hereditary ataxia  
Dementia in Parkinson's  
Chronic pain  
Panic disorder  
Attention deficit hyperactivity disorder  
Bipolar affective disorder  
Multiple sclerosis  
Frontotemporal dementia  
Obstructive sleep apnea  
Autism  
Schizophrenia  
Alzheimer's disease  
Asperger syndrome  
Huntington's disease  
Depressive disorder  
Right temporal lobe epilepsy  
Post traumatic stress disorder  
Progressive supranuclear palsy  
Left temporal lobe epilepsy  
Juvenile myoclonic epilepsy  
Meta-analysis of all disorders

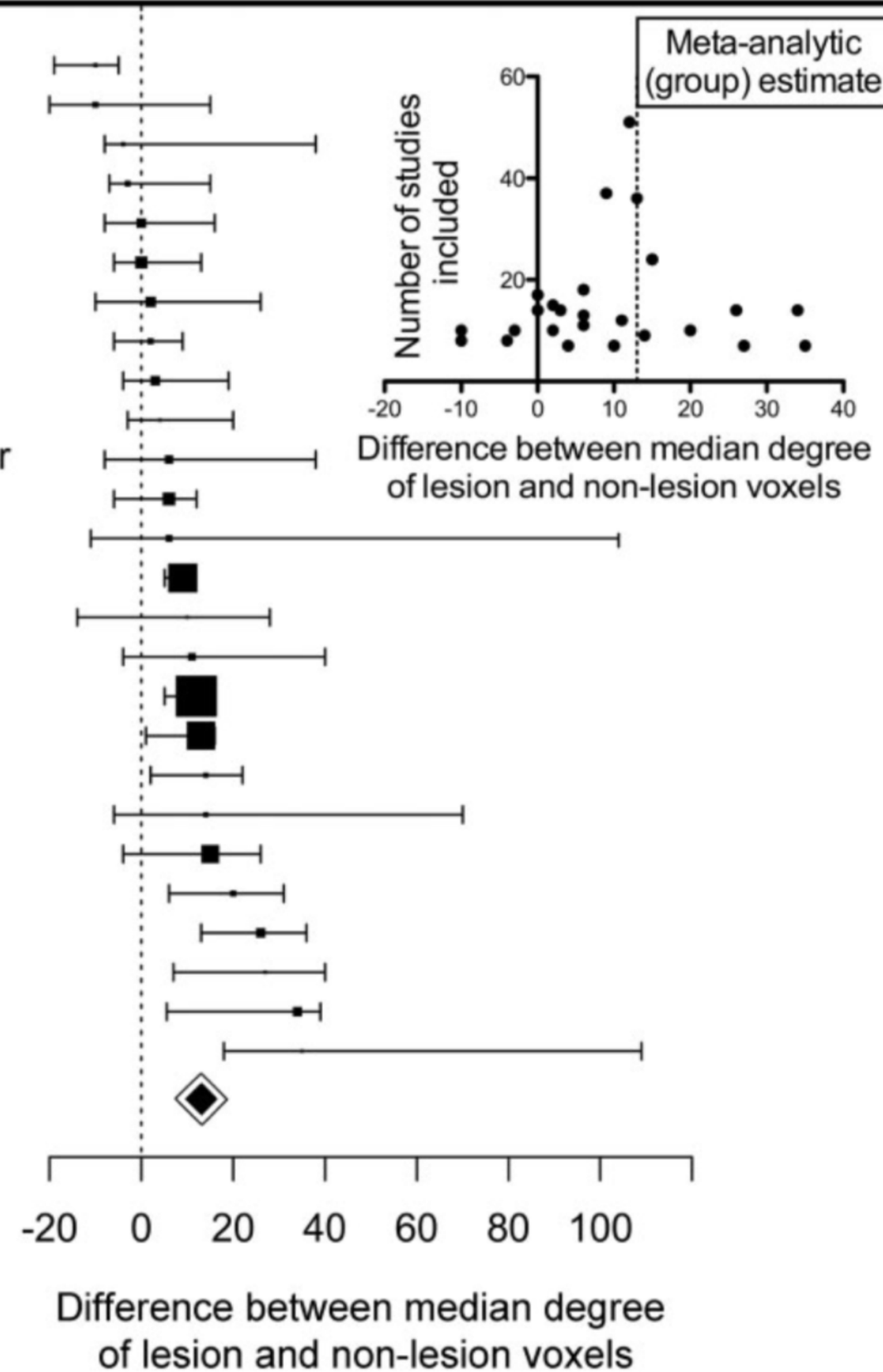


**Figure 6** Hub concentration of lesions is common to many specific brain disorders. For each of 26 disorders, box plots represent the difference in median degree of lesion voxels versus non-lesion voxels with a bootstrap 95% CI; the size of the box is proportional to the number of primary studies in the MRI literature. Small inset plot shows the relationship between sample size and difference in median degree for every study. Note that results from individual disorders are symmetrically distributed around the meta-analytical summary of all disorders, with a larger variance observed for disorders represented by fewer studies.

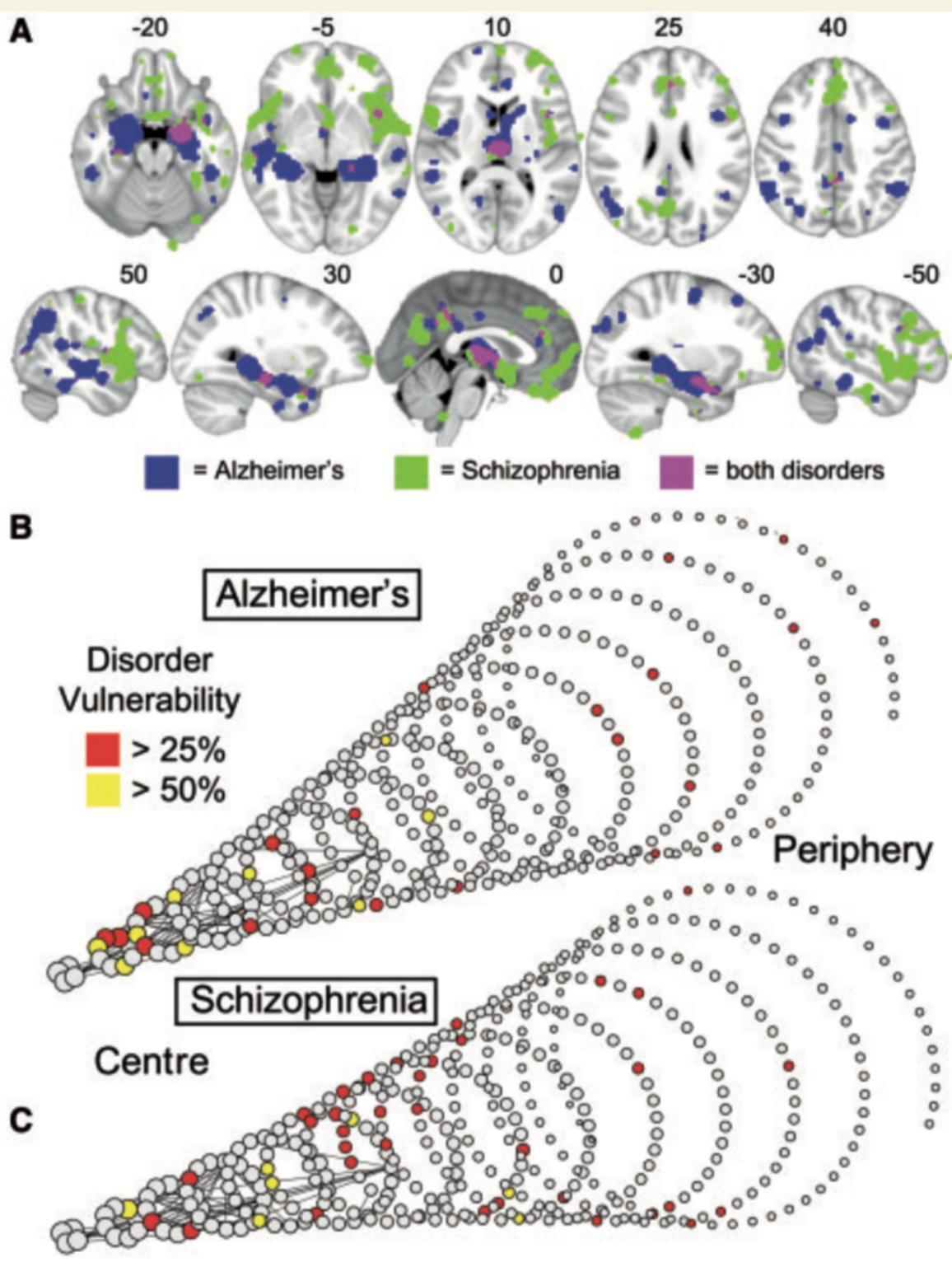


**Figure 7** Schizophrenia and Alzheimer's disease impact mainly on anatomically distinct subsets of hubs. **(A)** Meta-analytic maps of cortical and subcortical lesions associated with schizophrenia (green voxels), or Alzheimer's disease (blue voxels), or both disorders (pink voxels). **(B and C)** Lesions mapped in spiral networks in schizophrenia **(B)** and Alzheimer's disease **(C)** where the tip represents the highest degree nodes for both disorders and the strongest 0.1% of edges are shown.